Supporting information

Size-Controlled Hydrothermal Synthesis of Crystalline High-Entropy Spinel Oxide Nanoparticles for Oxygen Evolution Electrocatalysts

Ryoga Kato,†,‡ Kazuyuki Iwase,‡,* Hiroto Okuyama,# Akiko Tsurumaki, §,ᵹ Hitoshi Kasai,‡ Kouki Oka,‡ Takeo Yamaguchi# and Takaaki Tomai ‡,$

†: Department of chemical engineering, Graduate school of engineering, Tohoku University, 6-6-11-604 Aramaki-aza Aoba, Aoba-ku, Sendai 980-8579, Japan.

‡: Institute of Multidisciplinary Research for Advanced Materials, Tohoku University, 2-1-1 Katahira, Aoba-ku, Sendai, 980-8577, Japan

#: Laboratory for Chemistry and Life Science, Institute of Science Tokyo, R1-17, 4259 Nagatsuta-cho, Midori-ku, Yokohama, Kanagawa 226-8501, Japan

§: Department of Chemistry, Sapienza University of Rome, Piazzale Aldo Moro 5 00185, Rome Italy

ᵹ: Hydro-Eco Research Center, Sapienza University of Rome, Via A. Scarpa 16 00161, Rome Italy

$: The frontier research institute for interdisciplinary sciences, Tohoku university, 6-3 Aramaki Aoba, Aoba-ku, Sendai, Miyagi 980-0845, Japan

KEYWORDS: Hydrothermal synthesis, High-entropy oxides, Oxygen evolution reactions, Size control, Solution synthesis

Supporting figures and tables

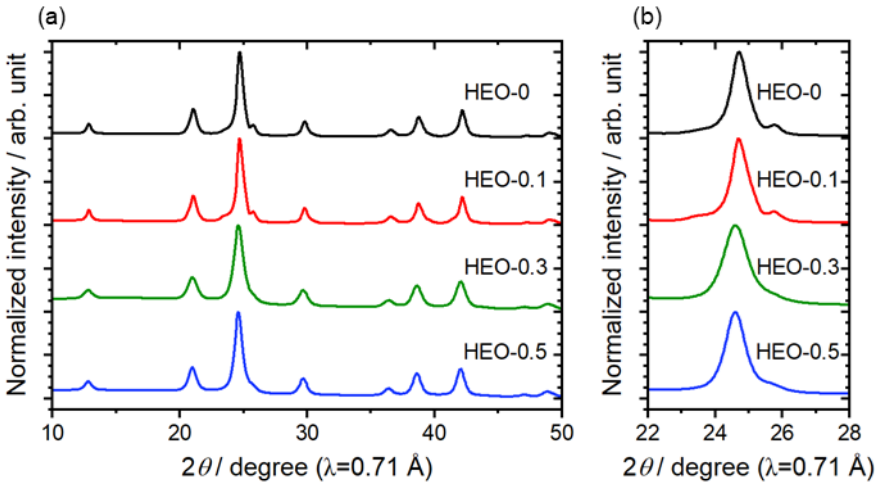

Figure S1 Synchrotron XRD patterns of HEO NPs with different catechol concentration. (a) Wide-angle view and (b) magnified view around the (311) peak.

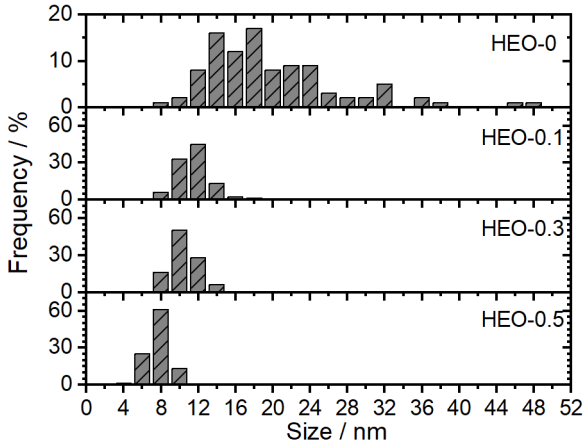

Figure S2 Particle size distribution calculated from TEM images. (a) HEO-0, (b) HEO-0.1, (c) HEO-0.3, (d) HEO-0.5. The size of 100 particles was counted from TEM images.

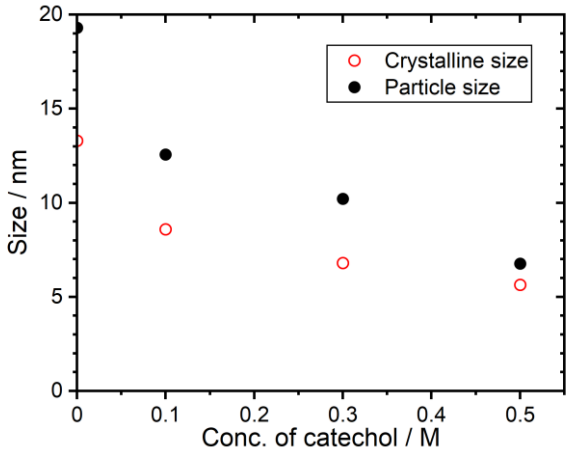

Figure S3 Crystallite size from XRD patterns and particle size from TEM images. The particle size was estimated by averaging the diameters of 100 particles observed from TEM images.

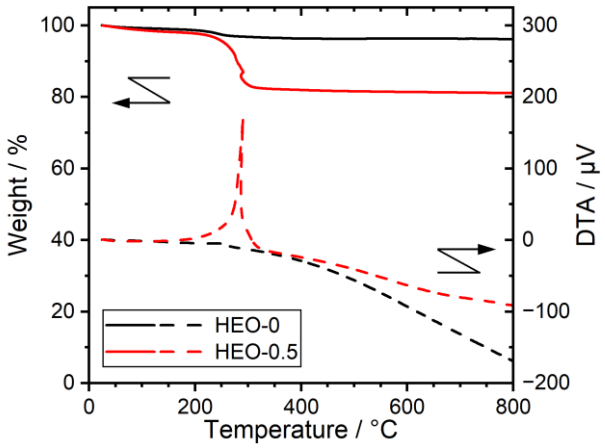

Figure S4 TG/DTA curves of HEO-0 and HEO-0.5. The solid line and the dashed line represent the weight of TG and the DTA signal, respectively. Black: HEO-0, Red: HEO-0.5.

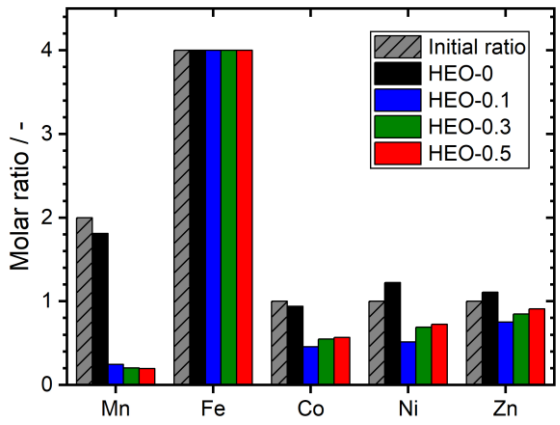

Figure S5 Metal element ratio of HEO NPs obtained by ICP-OES measurements. The Fe value is normalized as 4.

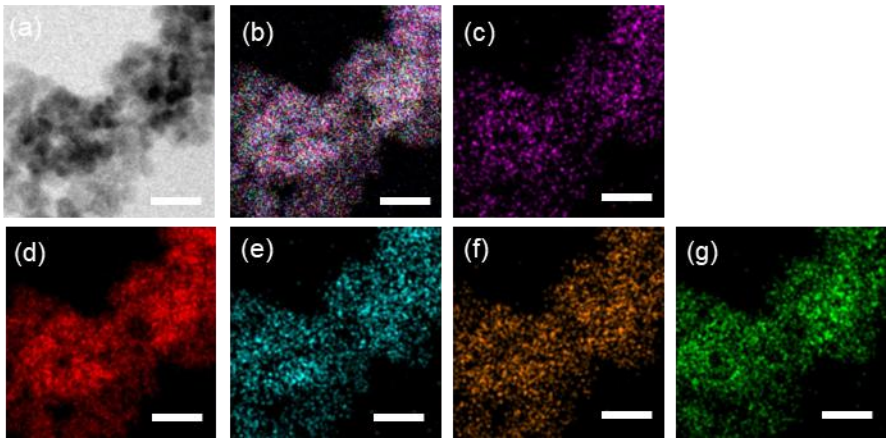

Figure S6 Wide range STEM images of HEO-0.5. (a) ABF image and (b-g) the corresponding EDX-mapping. (b) merge, (c) Mn, (d) Fe, (e) Co, (f) Ni and (g) Zn. The scale bar is 20 nm.

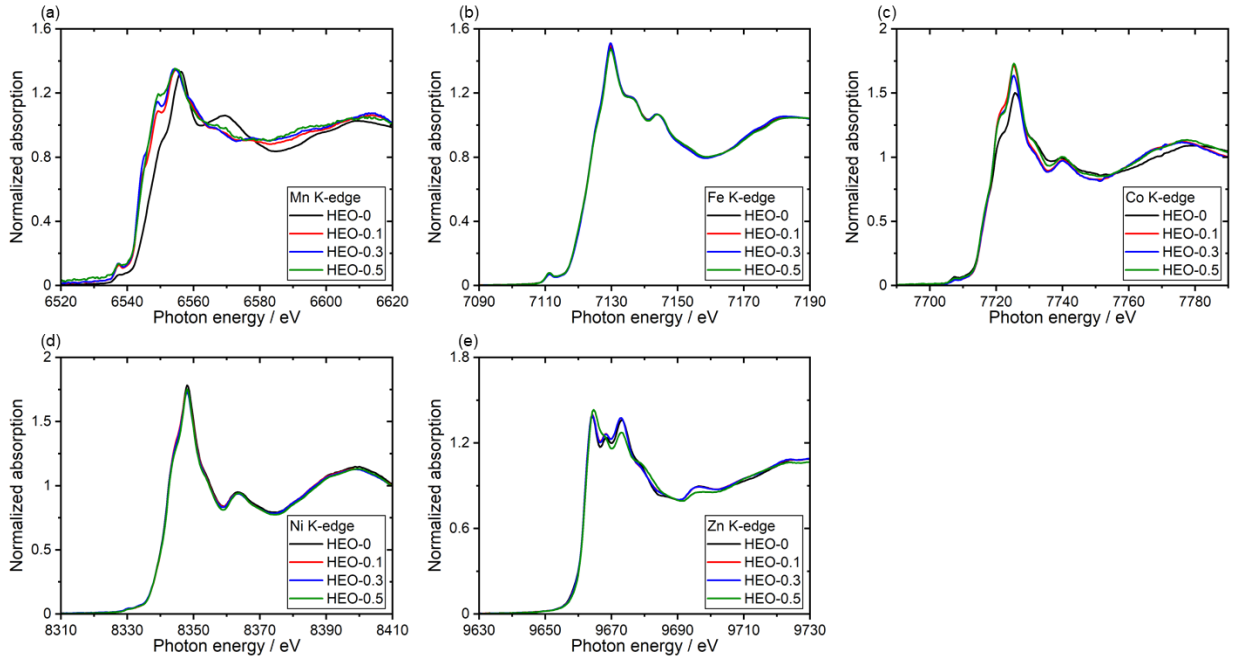

Figure S7 Metal K-edge XANES spectra of constituent metal elements of the HEO NPs. (a) Mn, (b) Fe, (c) Co, (d) Ni, and (e) Zn.

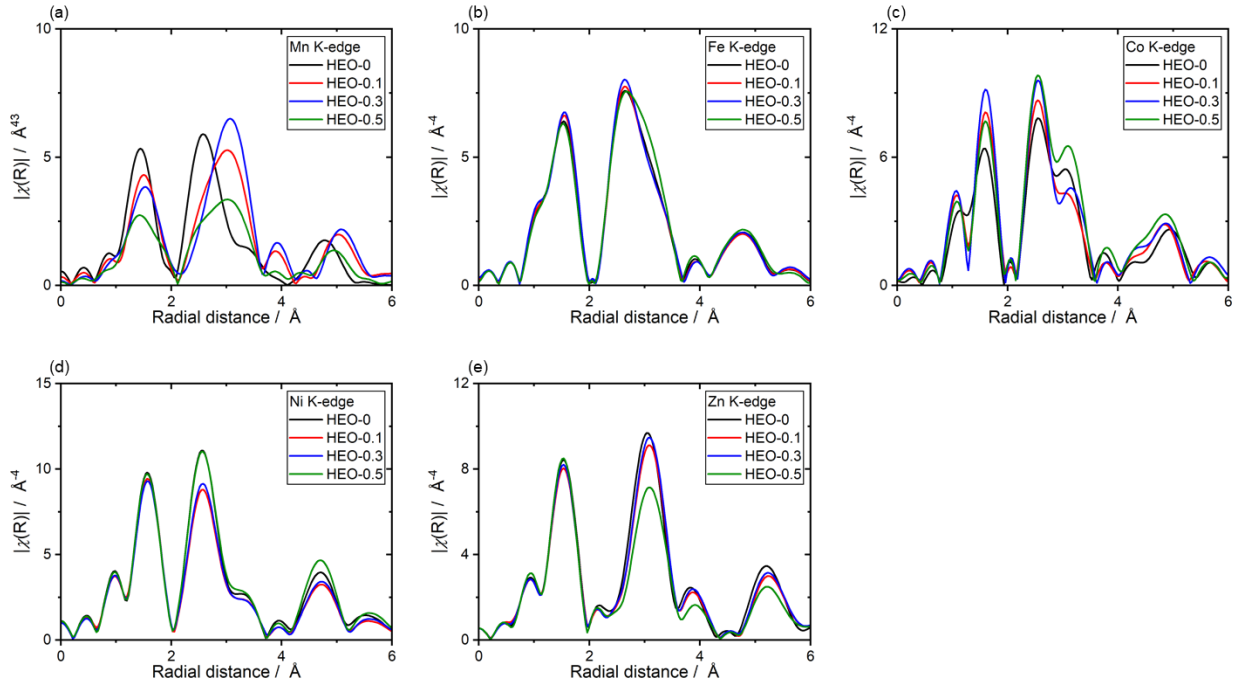

Figure S8 Metal K-edge FT-EXAFS spectra of constituent metal elements of HEO-NPs. (a) Mn, (b) Fe, (c) Co, (d) Ni, and (e) Zn.

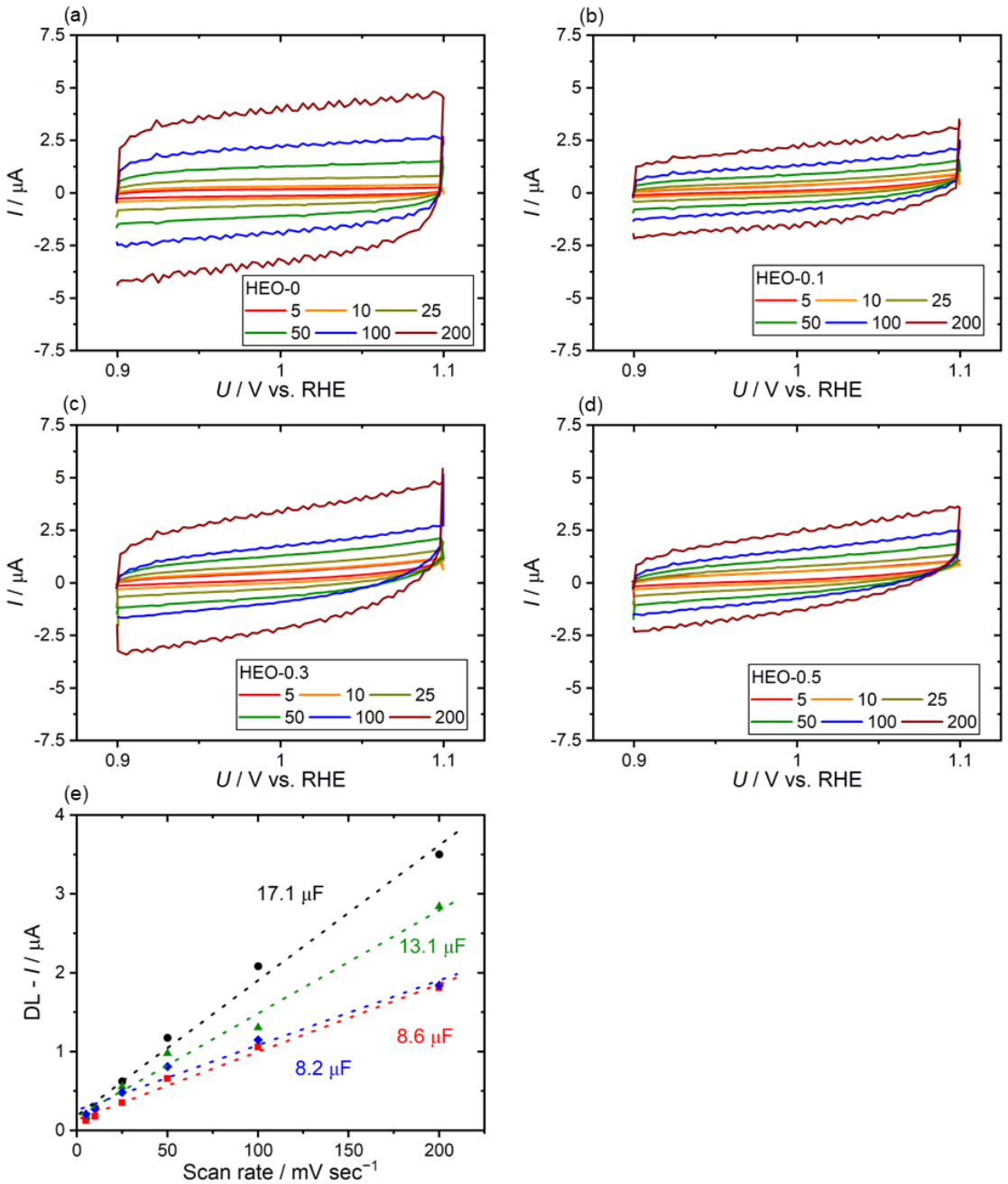

Figure S9 Evaluation of double-layer capacitance for CNT-free HEO electrodes. CVs of (a) HEO-0, (b) HEO-0.1, (c) HEO-0.3, and (d) HEO-0.5 recorded in a non-faradaic potential region between 0.9 and 1.1 V vs. RHE at scan rates of 5 – 200 mV s^{-1}. (e) Capacitive current plotted as a function of scan rate with the inset number calculated double layer capacitance (black: HEO-0, red: HEO-0.1, green: HEO-0.3, blue: HEO-0.5). The electrode was prepared modifying electrode with catalysts inks without CNTs in the same catalyst loading amount to exclude the electrochemical capacitance of CNTs.

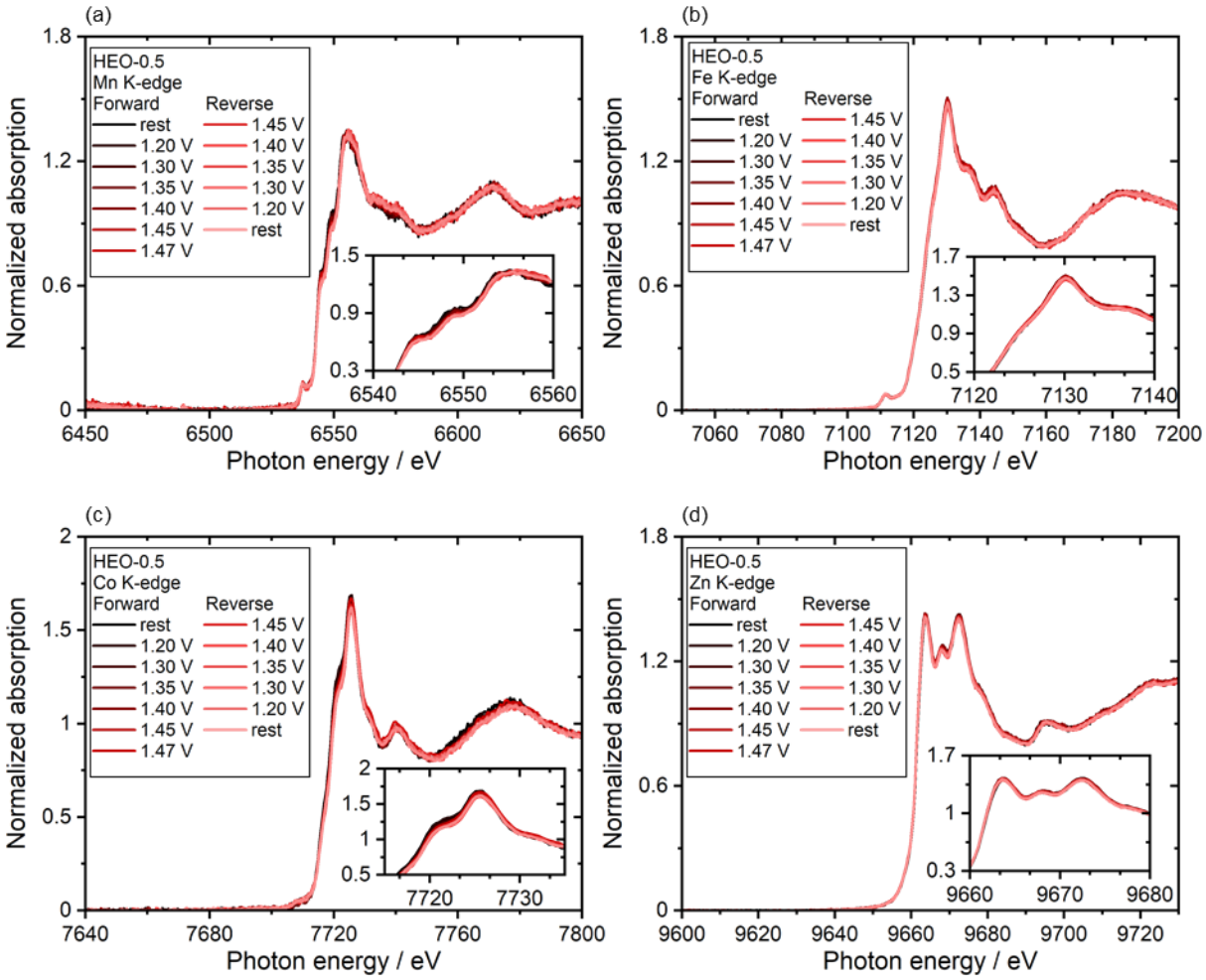

Figure S10 In-situ XANES spectra of the metal K-edge for the HEO-0.5 in the redox region. (a) Mn, (b) Fe, (c) Co and (d) Zn. The potential sweep is initially from 1.2 V to 1.47 V as the forward scan and go back to 1.2 V as the reverse scan.

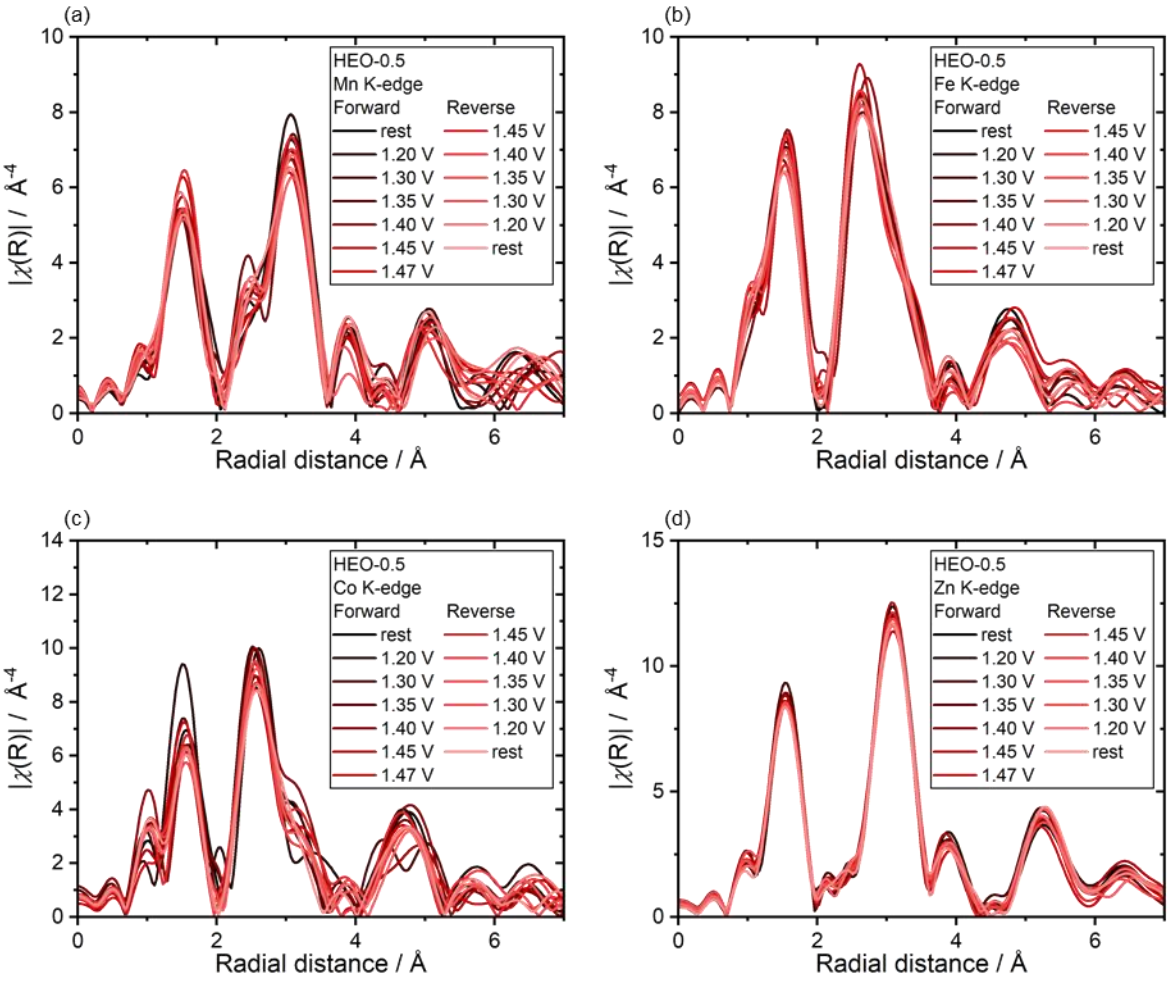

Figure S11 In-situ FT-EXAFS spectra of the metal K-edge for the HEO-0.5 in the redox region. (a) Mn, (b) Fe, (c) Co and (d) Zn. The potential sweep is initially from 1.2 V to 1.47 V as the forward scan and go back to 1.2 V as the reverse scan.

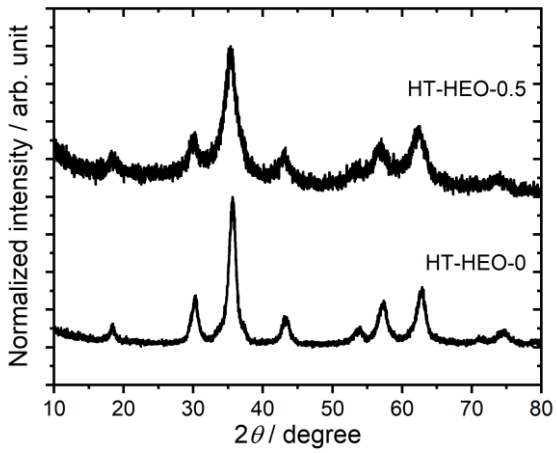

Figure S12 XRD patterns of HEO synthesized hydrothermal method with (HT-HEO-0.5) and without (HT-HEO-0) catechol. For the details of the synthesis protocol, see the experimental section.

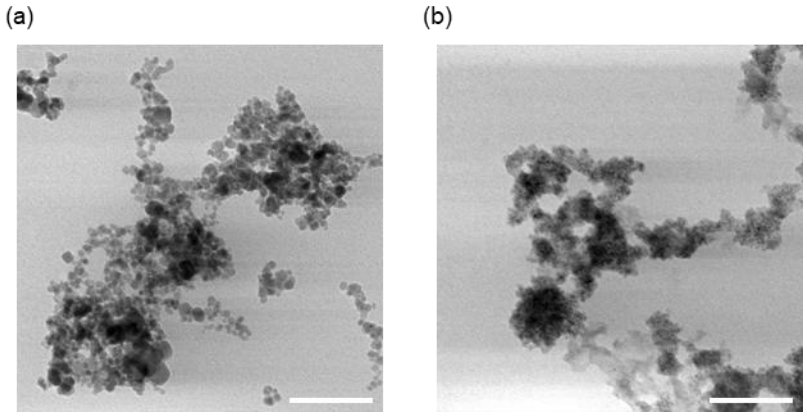

Figure S13 TEM images of HEO synthesized hydrothermal method. (a) HT-HEO-0 and (b) HT-HEO-0.5. The scale bar is 100 nm.

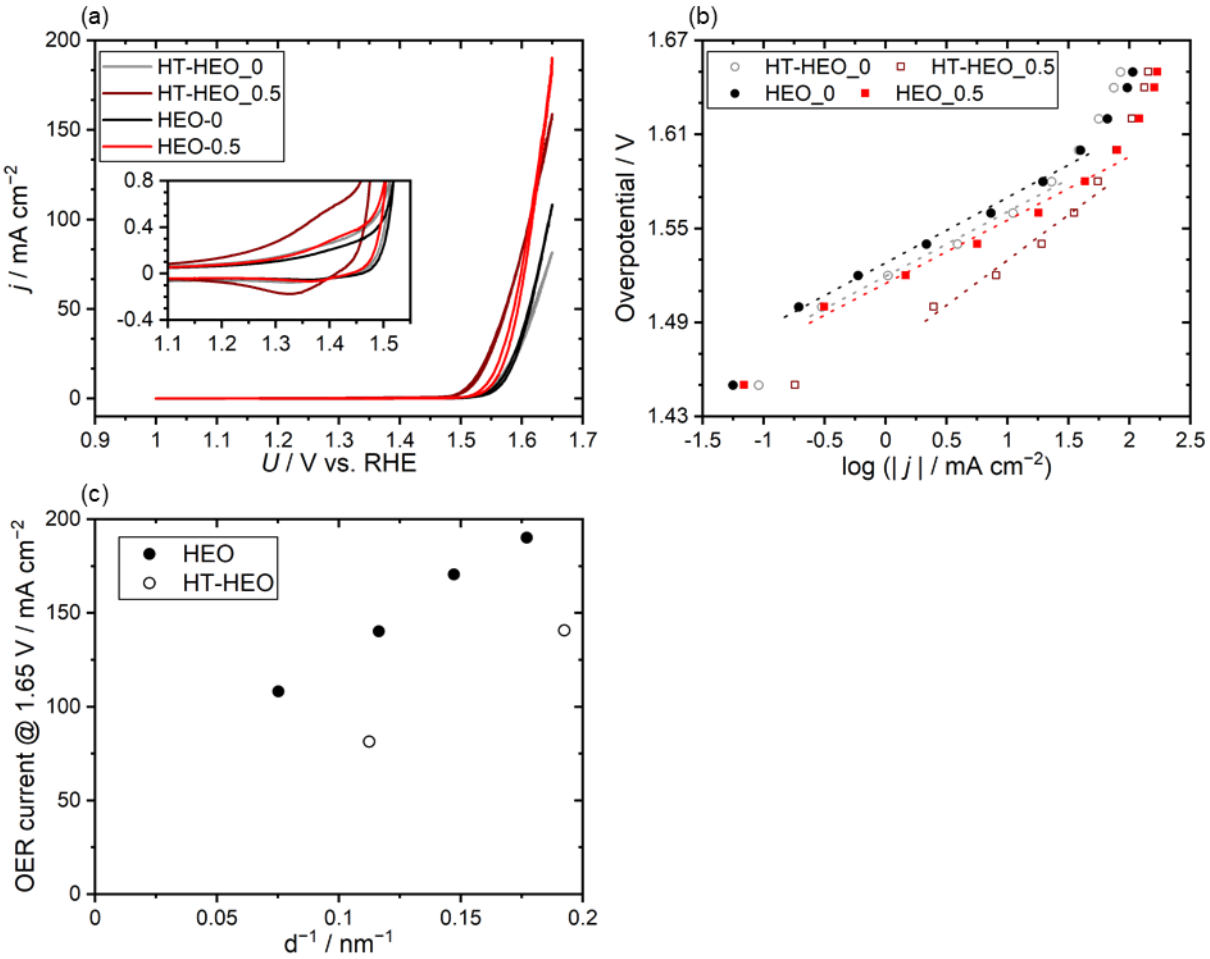

Figure S14 OER activity of HEO synthesized under hydrothermal method. The data of HEO catalysts are also shown for comparison. (a) Cyclic voltammograms of HEO NP, (b) Tafel plot of HEO NPs obtained by the chronoamperometric measurement, and (c) OER current at 1.65 V plotted against crystallite size obtained from XRD pattern.

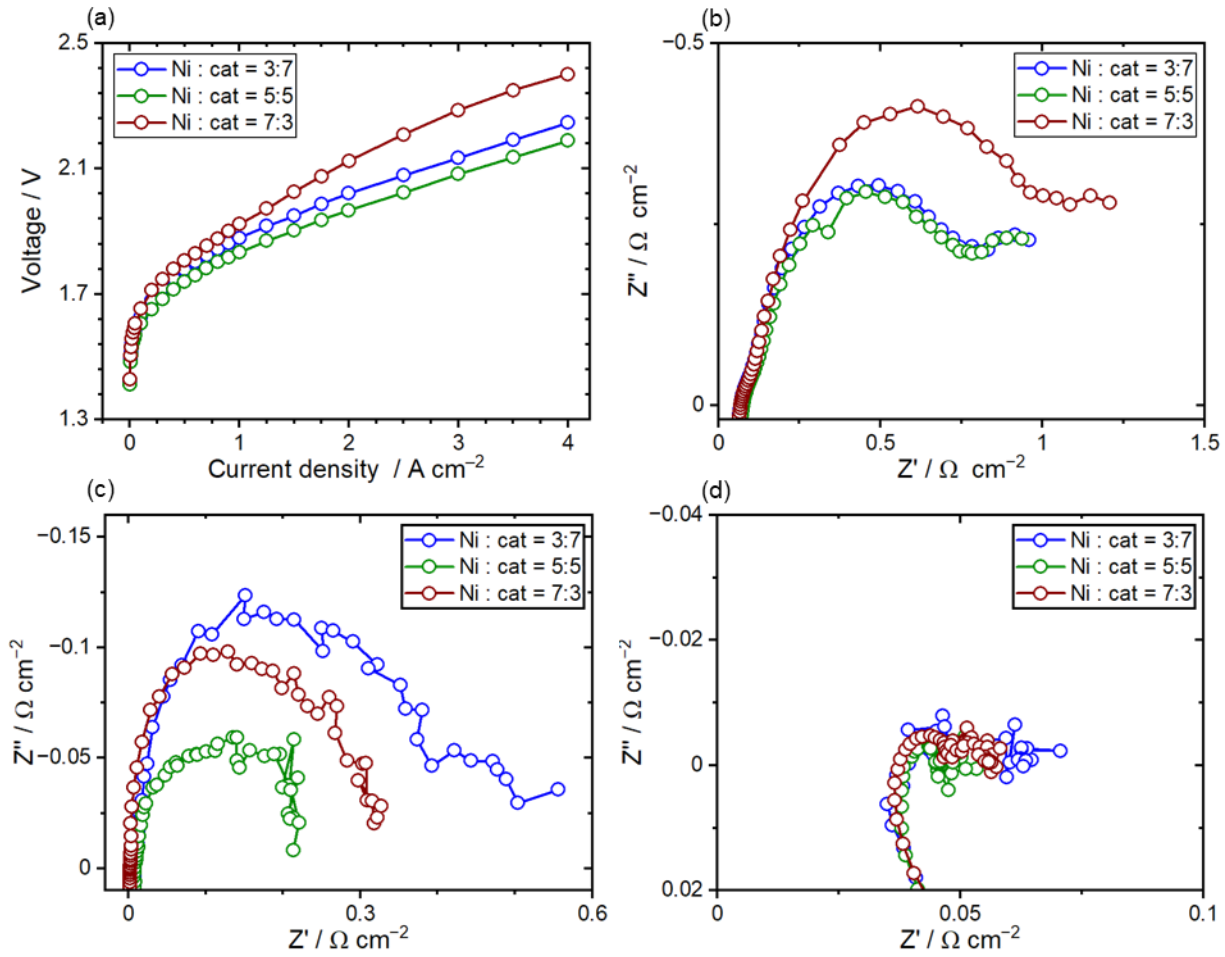

Figure S15 Polarization curves of AEMWE cells using HEO-0.5/Ni anodes with different Ni-HEO mass ratios in 1.0 M KOH at 80 °C. Corresponding Nyquist plots at 1.5 V applied potential for (b) the same MEAs, and Nyquist plots specifically for (c) anode and (d) cathode side contribution.

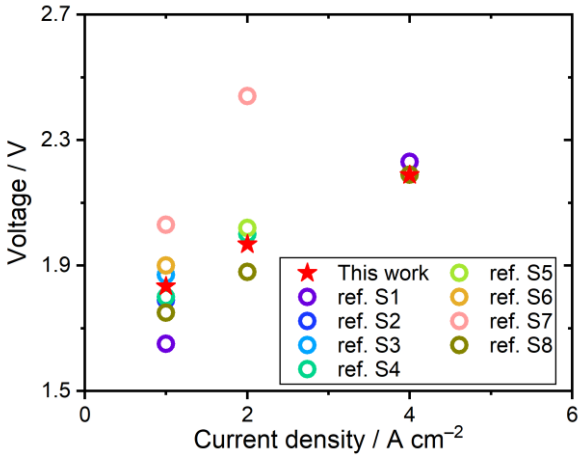

Figure S16 Comparison of the MEA performance using the developed catalyst in this study and previous studies listed in Table S2.

Table S1 Summarized table of the OER activities for reported spinel oxides evaluated using 1 M KOH solution. Overpotential is determined as the potential reaching 10 mA cm^{-2}.

Catalysts	Catalyst loading amount (mg/cm^2)	Particle size (nm)	Over-potential (mV)	Tafel slope value (mV/dec)	Ref.
HEO-0	179	19.3	342	37.7	This work
HEO-0.1	179	12.6	320	38.6	This work
HEO-0.3	179	10.2	323	37.3	This work
HEO-0.5	179	6.8	327	34.0	This work
HT-HEO-0	179	8.9[a]	340	37.8	This work
HT-HEO-0.5	179	5.2[a]	297	51.1	This work
NiFe-LDH	100	< 1μm (flower-like microspheres)	290	51	Ref. S9
CoOx	500	< 1μm (Nanoplate)	306	67	Ref. S10
CMO/NCNF	240	300 nm (nanofiber)	340	93.5	Ref. S11
Mp-Co_3O_4	138	80 nm (nanowire)	380	72	Ref. S12
N-CG-CoO	707	10-30 nm	340	71	Ref. S13

Note: The reference works used RDE composed of glassy carbon electrodes.
a: crystallite size is shown for HT-HEOI-0 and HT-HEO-0.5 since it is difficult to estimate the particle size from TEM images.

Table S2 Summarized table of the MEA characteristics tested in this study and reported paper.

Entry	Anode	Cathode	Membrane	Catalyst loading amount (mg/cm^2)	Activity	Condition	references
1	HEO-0.5-Ni	PrRu/C	PiperION 20 μm	0.6	1.83 V @ 1.0 A cm^{-2} 1.96 V @ 2.0 A cm^{-2} 2.19 V @ 4.0 A cm^{-2}	1.0 M KOH 80 °C	This work
2	Ni_2Fe_8–Ni_3S_2/NF	Ni_4Mo/MoO_2 /NF	FAA-3-50 50 μm	24.87	1.65 V @ 1.0 A cm^{-2} 2.23 V @ 4.0 A cm^{-2}	1.0 M KOH 80 °C	Ref. S1
3	NiFe-LDH	JH-Pt_2Tb/C	Sustainion X37-50 RT	2.0	1.79 V @ 1.0 A cm^{-2}	1.0 M KOH 80 °C	Ref. S2
4	NiFe-LDH	Ru-YNC	Sustainion X37-50 Grade 60	0.5	1.87 V @ 1.0 A cm^{-2}	1.0 M KOH 80 °C	Ref. S3
5	NiFe LDH	PtNiCoP@MXene	Sustainion X37-50 grade RT 50 μm	2.5	1.80 V @ 1.0 A cm^{-2} 2.00 V @ 2.0 A cm^{-2}		Ref. S4
6	$NiFe_2O_4$	NiFeCo	PiperION 15 μm	2.0	1.90 V @ 1.0 A cm^{-2} 2.02 V @ 2.0 A cm^{-2}	1.0 M KOH 80 °C	Ref. S5
7	NiFe-LDH/NF	Pt-AC/Cr-N-C	Sustainion X37-50	N/A	1.90 V @ 1.0 A cm^{-2}	1.0 M KOH 80 °C	Ref. S6
8	FeCoNiCrMn HEA/NM	FeCoNiCrMn HEA/NM	-	N/A	2.03 V @ 1.0 A cm^{-2} 2.44 V @ 2.0 A cm^{-2}	1.0 M KOH 80 °C	Ref. S7
9	FeCoNiMoW @FeCoNiOOH	PtRu/C	PiperION-A40-HCO3 40 μm	1.0	1.75 V @ 1.0 A cm^{-2} 1.88 V @ 2.0 A cm^{-2} 2.19 V @ 4.0 A cm^{-2}	1.0 M KOH 80 °C	Ref. S8

Supporting references

[S1] Ding, G.; Lee, H.; Li, Z.; Du, J.; Wang, L.; Chen, D.; Sun, L. Highly Efficient and Durable Anion Exchange Membrane Water Electrolyzer Enabled by a Fe–Ni3S2 Anode Catalyst. *Adv. Energy Sustain. Res.* 2022, 4 (1), 2200130.

[S2] Yan, W.; Mou, Y.; Li, M.; Ma, K.; Xu, Z.; Lu, T.; Du, H.; Wang, C.; Sun, H.; Chen, L.; et al. C15-Phase Platinum-Lanthanide Intermetallics for Efficient Hydrogen Evolution: Identifying Lanthanide's Enhanced Mechanism. *Adv. Mater*. 2025, 37 (34), 2506936.

[S3] Zhang, H.; Guo, H.; Zhang, F.; Zhang, J.; Cheng, Y.; Ma, Y.; Ma, L.; Qi, L. Cascade electrocatalysis via integration of ruthenium clusters and yttrium single atoms for a boosted alkaline hydrogen evolution reaction. *Energy Environ. Sci.* 2025, 18 (12), 6141-6153.

[S4] Niu, H. J.; Huang, C.; Sun, T.; Fang, Z.; Ke, X.; Zhang, R.; Ran, N.; Wu, J.; Liu, J.; Zhou, W. Enhancing Ni/Co Activity by Neighboring Pt Atoms in NiCoP/MXene Electrocatalyst for Alkaline Hydrogen Evolution. *Angew. Chem. Int. Ed*. 2024, 63 (20), e202401819.

[S5] Yassin, K.; Attias, R.; Tsur, Y.; Dekel, D. R. Identifying and Quantifying Loss Sources in Anion-Exchange Membrane Water Electrolyzers. *ACS Electrochemistry* 2025, 1 (5), 655-666.

[S6] Zeng, L.; Zhao, Z.; Huang, Q.; Zhou, C.; Chen, W.; Wang, K.; Li, M.; Lin, F.; Luo, H.; Gu, Y.; et al. Single-Atom Cr-N(4) Sites with High Oxophilicity Interfaced with Pt Atomic Clusters for Practical Alkaline Hydrogen Evolution Catalysis. *J. Am. Chem. Soc*. 2023, 145 (39), 21432-21441.

[S7] Zhang, Y.; Wan, Q.; Huang, L.; Jiang, T.; Wu, S.; Li, D.; Liu, Y.; Wu, H.; Ren, F. Bifunctional high-entropy alloy electrocatalysts for stable overall water splitting at industrial-level current densities. *J. Mater. Chem. A* 2025, 13 (23), 17384-17392.

[S8] Guo, L.; Huang, Y.; Qin, Y.; Chen, B.; Liu, C.; Chen, H.; Zhang, J.; Zhang, X.; Wang, Q. Self-reconstruction of FeCoNiMoW high entropy alloy to boost OER activity with robust stability for anion exchange membrane water electrolyzer. *Nanoscale* 2025, 17 (29), 17312-17323.

[S9] Zhong, H.; Liu, T.; Zhang, S.; Li, D.; Tang, P.; Alonso-Vante, N.; Feng, Y. Template-free synthesis of three-dimensional NiFe-LDH hollow microsphere with enhanced OER performance in alkaline media. *J. Energy Chem.* 2019, 33, 130-137.

[S10] Xu, W.; Lyu, F.; Bai, Y.; Gao, A.; Feng, J.; Cai, Z.; Yin, Y. Porous cobalt oxide nanoplates enriched with oxygen vacancies for oxygen evolution reaction. *Nano Energy* 2018, 43, 110-116.

[S11] Chen, X.; Yan, Z.; Yu, M.; Sun, H.; Liu, F.; Zhang, Q.; Cheng, F.; Chen, J. Spinel oxide nanoparticles embedded in nitrogen-doped carbon nanofibers as a robust and self-standing bifunctional oxygen cathode for Zn–air batteries. *J. Mater. Chem. A* 2019, 7 (43), 24868-24876.

[S12] Wang, Y.; Zhou, T.; Jiang, K.; Da, P.; Peng, Z.; Tang, J.; Kong, B.; Cai, W. B.; Yang, Z.; Zheng, G. Reduced Mesoporous Co3O4 Nanowires as Efficient Water Oxidation Electrocatalysts and Supercapacitor Electrodes. *Adv. Energy Mater.* 2014, 4 (16), 1400696.

[S13] Mao, S.; Wen, Z.; Huang, T.; Hou, Y.; Chen, J. High-performance bi-functional electrocatalysts of 3D crumpled graphene–cobalt oxide nanohybrids for oxygen reduction and evolution reactions. *Energy Environ. Sci.* 2014, 7 (2), 609-616.